Source of entangled atom pairs on demand using the Rydberg blockade

S. Wüster, S. Möbius, M. Genkin, A. Eisfeld, and J. M. Rost

Max-Planck-Institute for the Physics of Complex Systems, 01187 Dresden, Germany
(Received 27 September 2013; published 27 December 2013)

Two ultracold atom clouds, each separately in a dipole-blockade regime, realize a source of entangled atom pairs that can be ejected on demand. Entanglement generation and ejection is due to resonant dipole-dipole interactions, while van der Waals interactions are predominantly responsible for the blockade that ensures the ejection of a single atom per cloud. A source of entangled atoms using these effects can operate with a 10 kHz repetition rate producing ejected atoms with velocities of about 0.5 m/s. Using spatially resolved Rydberg state coupling and detection, a violation of Bell's inequalities could be measured in our setup.

I. INTRODUCTION

The interaction between alkali-metal atoms excited to Rydberg states is about 10 orders of magnitude stronger than in the ground state [1,2]. This can lead to a complete blockade of double excitation in a small volume [3,4], a drastic effect that can be exploited to engineer quantum gates [5,6], giant optical nonlinearities [7,8], and ultimately single-photon sources [9–11].

In a sufficiently tightly confined atomic gas, the blockade allows precisely one atom to carry a Rydberg excitation. This atom can then be selectively separated from the gas using external fields. Hence the blockade has also been proposed to realize single atom sources [9]. As we show here, the use of resonant dipole-dipole interactions for the ejection of atom pairs will generate entangled (Bell) pair states and also offers an elegant way to avoid perturbations of the parent atomic gas.

Our setup allows a replication of the spin variant [12] of the Einstein-Podolsky-Rosen paradox (EPR) [13], utilizing massive particles. Compared to continuous variables EPR experiments with optical fields, e.g., [14–19], there exist much fewer experimental realizations with massive particles [20–22]. This has motivated several recent theoretical proposals [23,24] in the active field of EPR entanglement [25].

Beyond the possible EPR source, the present atom source may have applications for atom-laser outcoupling [26,27], nanolithography [28], or controlled collisions in ultracold chemistry [29].

The essentials of our proposal are sketched in Fig. 1. The two tightly trapped atomic clouds have a separation d slightly larger than the blockade radius r_{bl} for a given principal quantum number ν of a Rydberg state. It is then possible to excite precisely one atom to a Rydberg state $|\nu,l\rangle$ in *each* cloud, where l is the orbital angular momentum. Initially we target the state $|s\rangle = |\nu,l\rangle$ with $l = 0$.

Subsequently, a suitable microwave (rf) pulse on the $|s\rangle \rightarrow |p\rangle$ transition, where $p = |\nu,l\rangle$ with $l = 1$, can excite the whole system to a collective state (exciton) with repulsive resonant dipole-dipole interactions between pairs of atoms from different clouds [30–35]. At separation d, this interaction will be much stronger than van der Waals interactions, and accelerates the atoms away from one another [36–38]. In the repulsive exciton, the electronic state of the ejected atom pair is a Bell state [37,38], hence our setup directly implements the EPR scenario [12]. Measuring EPR correlations requires

independent coupling between the $|s\rangle$ and $|p\rangle$ Rydberg states for the two ejected atoms. We discuss a possible realization of this coupling based on microwave resonators.

In practice, it is beneficial to set up the clouds with $d \lesssim r_{bl}$. In that case the detuning of the Rydberg excitation lasers has to compensate for the van der Waals interaction at distance d, in an antiblockade type setting [39]. We evaluate the performance of pulsed atom ejection under these conditions, and investigate the required atom excitation scheme in detail. To this end we employ an extension of Tully's quantum-classical surface hopping method [40,41] to allow an explicitly time-dependent Hamiltonian. We can then model the excitation and acceleration processes of the atoms in the same framework.

This article is organized as follows: In Sec. II we present our model and the methods needed for its solution. In Sec. III we use this method to simulate the ejection of an entangled atom pair from two traps, and determine key relations between system parameters and repetition rate. Later, in Sec. IV, we describe protocols to measure the violation of a Bell inequality [42,43] in the present setting. They also allow an experimental verification of entanglement transport based on the same Rydberg Bell states as those occurring here [37,38].

II. MODEL AND METHODS

Consider an assembly of $N = N_A + N_B$ neutral atoms of mass M located at positions r_n, restricted to one dimension and confined in two separate harmonic wells. This could be realized by trapping atoms in two sites of an optical lattice, not necessarily adjacent, or a double well trap. N_A atoms are localized in one of the wells, forming cloud A and N_B in the other well, forming cloud B. Near the centers of each well at $x = \pm d/2$, the potential is approximately harmonic: $V(r_n) = M\omega^2(r_n \pm d/2)^2/2$, and the atoms are initially in the Gaussian ground state of the trap with width $\sigma = \sqrt{\hbar/M\omega}$. Under the blockade conditions described in the Introduction, one expects that after Rydberg excitation only a single atom per trapping site undergoes significant motional dynamics, as we have shown previously [44]. If no real Rydberg states are accessed, but *all* ground states are off-resonantly dressed with Rydberg states [44], the system can evolve into a spatial mesoscopically entangled state through dipole-dipole interactions [45,46]. The present paper however does not consider the dressing scenario.
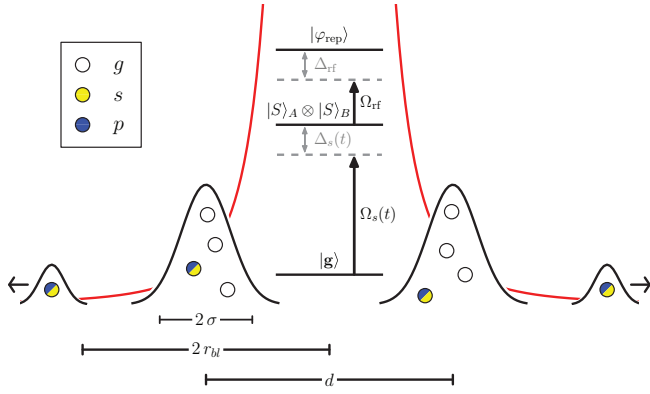
FIG. 1. (Color online) Schematic of twin atom clouds. Shown are the Rydberg blockade radius $r_{\rm bl}$, the cloud separation d, and width σ. The center shows the many-body level scheme and red lines symbolize the repulsive exciton potential. For simplicity d here is slightly larger than $r_{\rm bl}$, while for the scenario in Fig. 3 it is slightly smaller, as explained in the text. The two-color circles symbolize atom pairs in superposition states $|\Psi\rangle = (|sp\rangle + |ps\rangle)/\sqrt{2}$.

A. Hamiltonian and state space

We consider three essential states in ^{87}Rb atoms. A long lived ground state $|g\rangle$ and two Rydberg states $|\nu,l\rangle$, designated by $|s\rangle = |\nu,0\rangle$ and $|p\rangle = |\nu,1\rangle$. On these states we build the many-body basis $|\mathbf{k}\rangle \equiv |k_1,\ldots,k_{2N}\rangle \equiv |k_1\rangle \otimes \cdots \otimes |k_{2N}\rangle$, where $k_j \in \{S\} \equiv \{g,s,p\}$ describes the electronic state of atom j.

The state $|s\rangle$ is coupled to the ground state with Rabi frequency $\Omega_{\rm las}$ and detuning $\Delta_{\rm las}$ via a two-photon laser transition, and to the state $|p\rangle$ with (time dependent) Rabi frequency $\Omega_{\rm rf}$ and detuning $\Delta_{\rm rf}$ via a one-photon microwave transition. The resulting coupling between many-body states is sketched in Fig. 1 and will be explained shortly.

We formulate the many-body Hamiltonian

$$\hat{H} = \hat{H}_0 + \hat{H}_{\rm c} + \hat{H}_{\rm int}, \tag{1a}$$

$$\hat{H}_0 = \sum_{n=1}^{2N} \left[-\frac{\hbar^2}{2M} \nabla_{r_n}^2 + V(r_n,t)\hat{\sigma}_{gg}^{(n)} \right], \tag{1b}$$

$$\hat{H}_{\rm c} = \sum_n \left[\frac{\Omega_{\rm las}(t)}{2}\hat{\sigma}_{gs}^{(n)} + \frac{\Omega_{\rm rf}(t)}{2}\hat{\sigma}_{sp}^{(n)} + \text{H.c.} \right.$$
$$\left. - \Delta_{\rm las}(t)\hat{\sigma}_{ss}^{(n)} - [\Delta_{\rm rf}(t) + \Delta_{\rm las}(t)]\hat{\sigma}_{pp}^{(n)} \right], \tag{1c}$$

$$\hat{H}_{\rm int} = \sum_{nl} \left[D_{nl}\hat{\sigma}_{sp}^{(n)}\hat{\sigma}_{ps}^{(l)} + \sum_{a,b=s,p} W_{nl}^{(ab)}\hat{\sigma}_{aa}^{(n)}\hat{\sigma}_{bb}^{(l)} \right], \tag{1d}$$

with $\hat{\sigma}_{kk'}^{(n)} = |k_n\rangle\langle k'_n|$, where k_n, $k'_n \in S$. The operator $\hat{\sigma}_{kk'}^{(n)}$ acts only on the Hilbert space of atom n and is unity otherwise. In Eq. (1a), $\hat{H}_0$ describes the free motion of the atoms with coordinates r_n in the trapping potentials. Note that the trapping potential $V(r_n,t)$ only acts in the ground state, as typical magnetic or optical traps designed to trap ground state atoms are ineffective for Rydberg atoms [47]. $\hat{H}_{\rm c}$ contains the interaction of the atom with the laser (subscript las) and

the microwave radiation (subscript rf). Rabi frequencies are denoted by Ω and detunings by Δ. The last term $\hat{H}_{\rm int}$ is the interaction between atoms in Rydberg states, where $D_{nl}(\mathbf{R}) = D(|r_n - r_l|)$ describes transition dipole-dipole interactions between an atom in $|s\rangle$ and one in $|p\rangle$ and $W_{nl}^{(ab)} = W^{(ab)}(|r_n - r_l|)$ are van der Waals (vdW) interactions between atoms n and l with orbital quantum numbers $a,b = s,p$. The vector $\mathbf{R} = \{r_1,\ldots,r_N\}^T$ contains all atom coordinates.

In the following we will use the potentials $D(|r_n - r_l|) = C_3/|r_n - r_l|^3$ and $W(|r_n - r_l|) = C_6/|r_n - r_l|^6$, where $C_3 = \pm\mu^2$. The sign of C_3 depends on the explicit Rydberg states $|s\rangle$ and $|p\rangle$, while μ is the magnitude of the transition dipole between the latter. It will be important for the present work that $C_3 > 0$. The positive sign and the angular independence of $D(|r_n - r_l|)$ can be achieved by choosing the polarization axis of the microwave along the intercloud axis [38], which can reduce the dynamics to just a single selected total angular momentum m_j sublevel of the involved $|p\rangle$ state. Working with $s_{1/2}$ and $p_{3/2}$ states ensures $C_3 > 0$ [48], as required.

B. Numerical solutions

For flexible Rydberg systems, where atomic motion and excitation transport due to resonant dipole-dipole interactions affect each other, Tully's mixed quantum-classical approach [40,41,49] is convenient to apply and reliable [36–38,44,45]. Here we briefly review its core features to explain an extension required for the present work.

We propagate an electronic quantum state $|\Psi(t)\rangle = \sum_{\mathbf{k}} c_{\mathbf{k}}(t)|\mathbf{k}\rangle$ according to the usual time-dependent Schrödinger equation (TDSE)

$$i\hbar\frac{\partial}{\partial t}|\Psi(t)\rangle = \hat{H}_{\rm el}|\Psi(t)\rangle, \tag{2}$$

with electronic Hamiltonian $\hat{H}_{\rm el} = \hat{H}_{\rm c} + \hat{H}_{\rm int}$. The atomic motion is treated through a classical trajectory average with initial conditions drawn from the Wigner function of the lowest harmonic oscillator states within the two wells A and B.

Forces on the atoms arise from the harmonic trap and mutual interactions. Importantly, all these depend on the electronic state. In our algorithm these forces are always calculated as the gradient of *a single* selected Born-Oppenheimer surface $U_p(\mathbf{R})$. Surfaces are determined from the time-independent Schrödinger equation (TISE)

$$\hat{H}_{\rm el}|\varphi_n(\mathbf{R})\rangle = U_n(\mathbf{R})|\varphi_n(\mathbf{R})\rangle. \tag{3}$$

In the trajectory average, the surface index p that determines the motion of the atoms is allowed to stochastically switch to another one l. The switching probability is determined from the nonadiabatic coupling vector $\mathbf{d}_{pl} = \langle\varphi_l|\nabla\varphi_p\rangle$. Here we will additionally have transitions between different adiabatic surfaces due to the coupling to time-dependent electromagnetic fields. We take these into account with additional stochastic switches, due to the nonadiabatic coupling

$$t_{pl} = \langle\varphi_l|(\partial/\partial t)\varphi_p\rangle. \tag{4}$$

In order to conserve energy in a switch due to $\mathbf{d}_{pl}$ the velocity is appropriately adjusted along the direction of the nonadiabatic coupling vector $\mathbf{d}_{pl}$ [50]. For switches due to Eq. (4) there is

no adjustment, as for the duration of coupling pulses energy is not conserved.

III. PULSED ATOM EJECTION

In this section we sequentially describe the required steps for pulsed ejection of EPR entangled atom pairs from the twin atomic clouds sketched in Fig. 1. The simulated sequence here is fast enough to neglect atomic diffusion on the time scale of atom ejection, hence we set $V(r_n,t) = 0$ in Eq. (1a).

A. Excitation of blockade states

First we aim to excite a blockade state (also called superatom) in each cloud, so that the total state is $|S\rangle_A \otimes |S\rangle_B$, where $|S\rangle_X = \sum_{n \in X} |\pi_{n(s)}\rangle / \sqrt{N_X}$. We denote by $|\pi_{n(\alpha)}\rangle$ a state where all atoms are in $|g\rangle$, except atom n, which is in $|\alpha\rangle$, where $\alpha \in \{s,p\}$. The excitation could be achieved with a Rabi-π pulse in $\Omega_{\text{las}}(t)$, as long as the detuning Δ of the excitation field compensates the van der Waals interactions at distance d separating the clouds, thus $\Delta = C_6/d^6$. The detuning then allows us to excite one Rydberg atom in each cloud, despite them being separated by slightly less than the blockade radius, but would still ensure the absence of multiple excitations within one cloud. Since repeated use of the Rydberg atom source will decrease the number of remaining atoms per cloud N, the pulse durations have to be adjusted: The Rabi frequency between $|\mathbf{g}\rangle$, with all atoms in $|g\rangle$, and $|S\rangle_A$ is $\Omega_{\text{bl}} = \sqrt{N}\Omega_{\text{las}}(t)$.

Alternatively, repeated application of *identical* excitation sequences can be implemented by using a chirped adiabatic passage, as suggested in Ref. [51]. The frequency (detuning) $\Delta_{\text{las}}(t)$ of the effective laser coupling between $|g\rangle$ and $|s\rangle$ is adjusted from negative detuning to positive detuning in the course of a Gaussian envelope pulse for $\Omega_{\text{las}}(t)$. In this manner the state $|\mathbf{g}\rangle$ is adiabatically transformed into the state $|S\rangle_X$ in either cloud, regardless of N [52]. The symmetric chirp employed in Ref. [51] would have to be shifted by an offset $\Delta = C_6/d^6$.

Here we will employ Gaussian pulses with fixed detuning instead of chirped pulses, resulting in a larger repetition rate.

B. Excitation of repulsive exciton

Next, we transfer the two Rydberg excited atoms to a repulsive exciton state $|\varphi_{\text{rep}}\rangle = (|sp\rangle + |ps\rangle)/\sqrt{2}$ [44] via microwave coupling. In the same manner that we described in Ref. [45], the symmetric repulsive exciton state on a pair of atoms is adiabatically connected with the pair-state $|ss\rangle$, if an initially detuned microwave pulse on the $|s\rangle \leftrightarrow |p\rangle$ transitions is chirped from large positive detuning to zero detuning. Since the microwave usually couples with equal phases to all atoms, for interatomic distances much less than the wavelength, we can only directly access symmetric exciton states in this manner. This explains our choice $C_3 > 0$ in Sec. II A, for which the symmetric state is repulsive. The rf pulse shapes will be presented later. The final many-body state after the rf chirp will be $|\Psi_{\text{rep}}\rangle \equiv (|S\rangle_A \otimes |P\rangle_B + |P\rangle_A \otimes |S\rangle_B)/\sqrt{2}$.
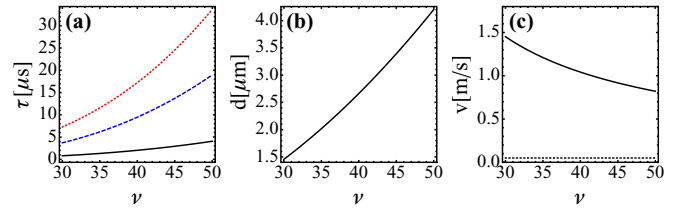

FIG. 2. (Color online) Characteristic features of our scheme as a function of principal Rydberg quantum number ν for Rb atoms. (a) Acceleration time τ_{acc} (solid black), overall time scale of motion $\tau_{\text{acc}} + \tau_{\text{drift}}$ (dashed blue), and life-time τ_{life} [54] (dotted red). (b) Cloud separation d. (c) Final velocity v_{fin} (solid) and recoil velocity v_{rec} (dotted) (see Sec. III D). See footnote [53] for definitions of the quantities above. For lighter atoms such as Li, the ratio between life time and motional time becomes much larger.

C. Atom ejection

After one atom in each cloud has been excited to a Rydberg state, and subsequently the Rydberg pair was transferred to a repulsive pair state for resonant dipole-dipole interactions, these interactions will ultimately push the excited atoms far enough away from their parent clouds to lift the blockade condition and allow the excitation of the next pair of Rydberg atoms.

For a given principal quantum number ν, the time scale of mechanical acceleration can be minimized by placing the two atom clouds as close as possible. We fix the intercloud distance d to $d = 0.65 r_{\text{bl}}$, where $r_{\text{bl}} = (C_6/\Omega_{\text{las}})^{1/6}$ is the van der Waals blockade radius. Significantly closer distances would invalidate our effective state model. In order for the last ejected pair of Rydberg atoms to no longer have significant resonant dipole-dipole interactions with subsequently excited atom pairs, they have to travel a distance greater than d away from their parent cloud. The time scale required is given by the distance d divided by the final velocity $v_{\text{fin}} = \sqrt{2\mu^2/(Md^3)}$, where μ^2/d^3 is the initial dipole-dipole interaction energy. Inserting the relation between d and the principal quantum number ν which arises from $d \sim r_{\text{bl}}$ we find that the motional time scales like $\nu^{31/12}$ [53]. Fast repetition rates thus favor *smaller* principal quantum numbers. In Fig. 2 we show the times required for acceleration and motion, compared to the pair lifetime, as a function of the principal quantum number ν.

D. Atom deexcitation

The measurement of the entanglement of EPR pairs, as discussed in Sec. IV, may benefit from the atoms being in a Rydberg state by using state selective field ionization [55–57] to infer pseudospin states. Alternatively, if one prefers long lived entanglement, one can deexcite the Rydberg atoms to two different long lived ground states $|s\rangle \to |g\rangle$, $|p\rangle \to |h\rangle$ (see also [58]). These could be members of the ground hyperfine multiplet $|F,m_F\rangle$, where F is the total angular momentum and m_F is the associated magnetic quantum number, for example $|g\rangle = |1,-1\rangle$ and $|h\rangle = |2,1\rangle$. A further advantage of controlled deexcitation is to avoid uncontrolled atomic recoil due to spontaneous emission from the atoms ejected by the source, for cases where a directed atomic beam is desirable. Even if

the atom incurs a recoil, it gains a velocity $v_{rec} = E(\nu)/(Mc)$ of about 0.04 m/s for Rydberg states of Rb. In the expression for v_{rec}, the speed of light is c and the energy difference to the ground state $E(\nu) \approx 13.6$ eV. Compared to a directed drift velocity due to dipole-dipole interactions, of the order of 0.5 m/s the recoil is thus relatively small, see Fig. 2(c).

E. Minimal model demonstration

The least number of atoms with which one can demonstrate essential features of the atom pair production is $N_A = N_B = 2$. This is done in the following, modeling Rydberg excitation and acceleration for 2 rubidium atoms per cloud, for $d = 3\,\mu$m, $\sigma = 0.3\,\mu$m, $\nu = 42$, which results in $\mu = 1715$ a.u. Atoms are subjected to a laser pulse followed by an rf chirp, separated by 1 μs wait time. The total electronic wave function in this section will be written as

$$|\Psi(t)\rangle = \sum_{n_1,n_2:n_3,n_4} c_{n_1,n_2:n_3,n_4}(t)|n_1 n_2 : n_3 n_4\rangle, \quad (5)$$

with $n_i \in \{g,s,p\}$. The electronic basis states $|n_1 n_2 : n_3 n_4\rangle$ are a more explicit notation for the $|\mathbf{k}\rangle$ in Sec. II A. Indices to the left of the colon label atom one and two, in cloud A, those to the right atom three and four, in cloud B. We take vdW interactions (regularized at some maximum value) into account to ensure a blockade for the propagation of the electronic states in Tully's algorithm, however, for the mechanical motion of atoms vdW forces can be neglected here [59].

The results are shown in Fig. 3. The total atomic density from the trajectory average [Fig. 3(a)] shows the two parent clouds and the ejection of an atom pair. While precisely one atom is ejected from each cloud, the underlying quantum state is a superposition of all combinations of atom pairs being ejected [44]. The electronic state populations are shown in Fig. 3(c), grouped into the absolute ground state $n_g = |c_{gg:gg}|^2$, single Rydberg excited states $n_s = |c_{sg:gg}|^2 + |c_{gs:gg}|^2 + |c_{gg:sg}|^2 + |c_{gg:gs}|^2$, doubly Rydberg excited states $n_{ss} = |c_{sg:sg}|^2 + |c_{sg:gs}|^2 + |c_{gs:sg}|^2 + |c_{gs:gs}|^2$ (due to the blockade more than one excitation per cloud is not permitted), and doubly Rydberg excited states, including one p excitation: $n_{sp} = |c_{sg:pg}|^2 + |c_{sg:gp}|^2 + |c_{gs:pg}|^2 + |c_{gs:gp}|^2 + |c_{pg:pg}|^2 + |c_{pg:gp}|^2 + |c_{gp:pg}|^2 + |c_{gp:gp}|^2$. The populations indicate almost perfect conversion, first from the state $|\mathbf{g}\rangle$, with all atoms in $|g\rangle$, to the blockade state via the chirped laser coupling, then from a blockade state in each cloud to a many-body repulsive exciton. This state is a superposition where each possible pair of one atom from cloud A and one from cloud B is with equal probability in the repulsive exciton state $|\varphi_{rep}\rangle = (|sp\rangle + |ps\rangle)/\sqrt{2}$.

The transitions in the electronic space lead to the correct fraction of ejected atoms, as shown in Fig. 3(b), hence adding nonadiabatic transitions according to Eq. (4) to the surface hopping algorithm is appropriate.

Finally, the figure also shows the shape of the laser and rf pulses and their respective frequencies, precise parameters are listed in [52].

As explained in [44], the physics presented in this section remains unchanged if we begin with many more atoms than the $N = 4$ modeled here, as long as the assumption of a full blockade of each cloud, but completely lifted blockade from
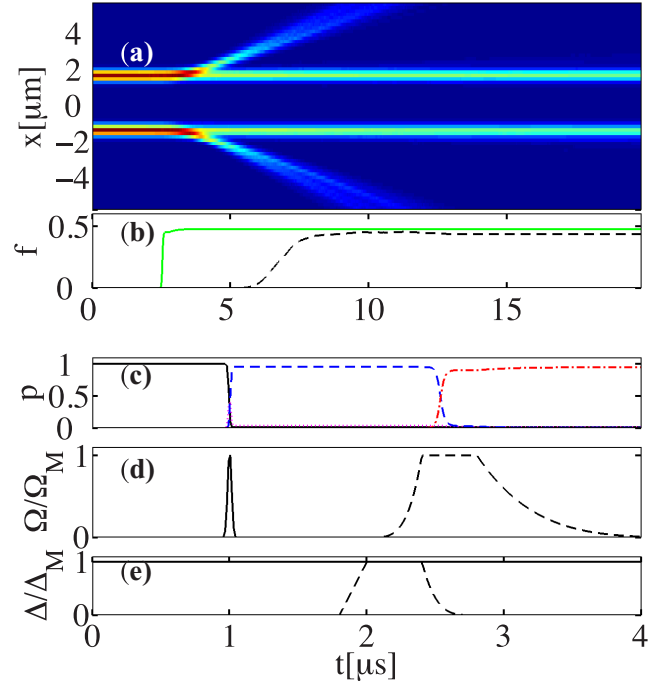

FIG. 3. (Color online) Ejection of an entangled Rb atom pair from two harmonic traps, using a quantum-classical model with 1024 stochastic trajectories. The principal quantum number is $\nu = 42$. (a) Total atomic density. (b) Fraction f of atoms ejected from the clouds (dashed black line), and population in the repulsive exciton state $n_{rep} = |\langle\Psi_{rep}|\Psi(t)\rangle|^2 = n_{sp}$ (green line). (c) Electronic populations during the first laser and r.f. pulse. In order of their dominance in time: (solid black) ground-state n_g, (dotted magenta) single Rydberg state n_s, (blue dashed) double Rydberg state n_{ss}, (red dot-dashed) Rydberg s and p state n_{sp}. See text for the definition of the populations $n_{g,s,ss,sp}$. (d) Laser (solid line) and microwave (dashed line) Rabi frequencies, normalized by their peak value Ω_M. For more details see [52]. (e) The same for detunings.

one cloud to the other is fulfilled. Repeated application of identical outcoupling sequences as in Fig. 3 then leads to a pulsed beam of single atoms, pairwise EPR entangled between two different beams.

Let us complete this section with an outlook on possible variants of atom ejection using dipole-dipole interactions. *Variant (i):* Instead of exciting $|s\rangle$ Rydberg states in both clouds and subsequently accessing $|p\rangle$ via microwave transitions, one could also excite atoms in cloud A to $|s\rangle$ and in cloud B to $|p\rangle$. The resulting exciton state is a superposition of repulsive and attractive dynamics, so that the atoms are ejected *toward each other* in 50% of the cases. Postselecting only the repulsive ones yields the same entanglement structure as in our original scheme. *Variant (ii):* One could excite $|s\rangle$ Rydberg states in both clouds, and subsequently admix population from neighboring ν manifolds via a $|ss\rangle \leftrightarrow |pp'\rangle$ Förster resonance [60–62]. Accessing the exciton proceeds via ramps of a static electric field here, instead of microwave pulses. Atoms in this case form entangled two-body states of the schematic form $\mathcal{N}(|ss\rangle + c_p|pp'\rangle)$, where $\mathcal{N}$ is a

normalization factor and $|c_p|^2 < 1$ depends on the Förster defect.

IV. ENTANGLEMENT MEASUREMENTS

There have been numerous theoretical proposals and experimental demonstrations of the EPR scenario [25]. While the original "Gedankenexperiment" relied on the measurement of position and momentum of spatially separated entangled particles, there have been successful experiments utilizing both continuous variables (CV) and discrete quantum states (spin-EPR) for the EPR paradox demonstration, as already briefly mentioned in the Introduction. CV experiments often rely on measurements of the amplitude and phase quadratures of optical fields, as first shown in Ref. [14]. However, even a test of entanglement in actual position and momentum of single photons is within experimental reach [63]. Overall, experiments with optical fields are known for their high detection efficiency, providing unequivocal EPR signatures, albeit with massless particles. Recently, however, the concept of CV-EPR was realized for massive particles, employing homodyne detection techniques [22].

The proposal described in the present work belongs to the spin-EPR category, utilizing massive particles (atoms) and discrete states. There have been successful experiments demonstrating EPR with atoms [20], ions [21], and mesoscopic atomic ensembles [64], along with further recent theoretical proposals for Bose-Einstein condensates [23,24]. We add a scenario in the realm of ultracold Rydberg physics. Such experiments can make use of single-atom detection techniques, based on strong interactions or field sensitivity of Rydberg states [65–67].

Concentrating on the ejected entangled atoms, the setup shown in Fig. 1 largely resembles the variant of the EPR paradox proposed by Bohm and Aharonov [12]. The Bohm and Aharonov scheme is based on the decay of a spin 0 particle into a pair of spin 1/2 particles in a spin singlet state of the form $|\Psi_S\rangle = (|\uparrow\downarrow\rangle - |\downarrow\uparrow\rangle)/\sqrt{2}$. Let us denote these particles by a and b. The measurable correlation between spin projections along axis $\mathbf{a}$ for particle a and $\mathbf{b}$ for particle b is expressed as

$$C_S^{(\mathbf{a},\mathbf{b})} = \langle \Psi_S | \boldsymbol{\sigma}_a \cdot \mathbf{a} \ \ \boldsymbol{\sigma}_b \cdot \mathbf{b} | \Psi_S \rangle = -\mathbf{a} \cdot \mathbf{b}. \quad (6)$$

Here $\boldsymbol{\sigma}_j$ is a vector of Pauli spin matrices acting in the spin space of atom j and $\mathbf{a} \cdot \mathbf{b}$ denotes the scalar product between the vectors $\mathbf{a}$ and $\mathbf{b}$.

By identifying electronic states with spin states according to $|s\rangle \to |\uparrow\rangle$, $|p\rangle \to |\downarrow\rangle$ (or if we work with deexcited ground states, Sec. III D, $|g\rangle \to |\uparrow\rangle$, $|h\rangle \to |\downarrow\rangle$), we can view the ejected atoms as a coupled spin-1/2 system. However, straightforward rf excitation of the repulsive exciton requires it to have the form $|\varphi_{\text{rep}}\rangle = (|sp\rangle + |ps\rangle)/\sqrt{2}$, which in the spin picture corresponds to a member of the triplet. In this triplet state $|\Psi_T\rangle = (|\uparrow\downarrow\rangle + |\downarrow\uparrow\rangle)/\sqrt{2}$ we obtain [68]

$$C_T^{(\mathbf{a},\mathbf{b})} = \langle \Psi_T | \boldsymbol{\sigma}_a \cdot \mathbf{a} \ \ \boldsymbol{\sigma}_b \cdot \mathbf{b} | \Psi_T \rangle = \mathbf{a} \cdot \mathbf{b} - 2a_z b_z \quad (7)$$

for the correlation, where a_i, b_i are the Cartesian components of the vectors $\mathbf{a}$ and $\mathbf{b}$.

In both, singlet and triplet cases, essential nonclassical features of entanglement are evident if one can violate a Bell

inequality [42], for example the CHSH form [43]

$$\bar{C} \equiv \left| C_T^{(\mathbf{a},\mathbf{b})} + C_T^{(\mathbf{a},\mathbf{b}')} + C_T^{(\mathbf{a}',\mathbf{b})} - C_T^{(\mathbf{a}',\mathbf{b}')} \right| \leqslant 2, \quad (8)$$

for any choice of axes $\mathbf{a}$, $\mathbf{a}'$, $\mathbf{b}$, $\mathbf{b}'$. All classical, realistic, local, hidden variable theories would have to fulfill Eq. (8).

If we wish to realize a violation of Eq. (8) using the emitted pair of Rydberg atoms, we thus should be able to independently control the measurement axes $\mathbf{a}$, $\mathbf{a}'$, $\mathbf{b}$, $\mathbf{b}'$. However, as we can only measure the angular quantum number of the outgoing Rydberg atoms—corresponding in the spin picture to a measurement of the z component—we cannot directly access the nonclassical region. This problem can be solved by coupling the $|s\rangle$ and $|p\rangle$ states for each of the emitted atoms to each other prior to the Rydberg state measurement. Let V_c ($c = a,b$) denote the respective coupling strengths and τ the coupling duration. The corresponding Hamiltonian for a single atom in the basis ($|s\rangle$, $|p\rangle$) thus reads

$$H_c = \begin{pmatrix} 0 & V_c \\ V_c & 0 \end{pmatrix}, \quad (9)$$

and the time evolution operator is given by

$$\begin{aligned} U_c &= \exp(-i H_c \tau) \\ &= \begin{pmatrix} \cos(\theta_c/2) & -i\sin(\theta_c/2) \\ -i\sin(\theta_c/2) & \cos(\theta_c/2) \end{pmatrix}, \end{aligned} \quad (10)$$

where $\theta_c = 2V_c\tau$. Note that the coupling is applied to each of the two atoms individually, hence we can write the full time evolution operator for the two-atom system as $U = U_a \otimes U_b$. Consider now some arbitrary initial two-particle state $|\chi\rangle$. One can easily verify that a z-component measurement for this state *after* the coupling period (at $t = \tau$) is equivalent to a correlation measurement such as in Eqs. (6) and (7) *before* the coupling period (at $t = 0$), where the two axes $\mathbf{c} = \mathbf{a},\mathbf{b}$ are given by

$$\mathbf{c} = [0, \sin(\theta_c), \cos(\theta_c)]^T, \quad (11)$$

i.e., the following equality holds:

$$\langle \chi | \boldsymbol{\sigma}_a \cdot \mathbf{a} \ \ \boldsymbol{\sigma}_b \cdot \mathbf{b} | \chi \rangle = \langle \chi | U^\dagger \sigma_a^z \ \ \sigma_b^z U | \chi \rangle. \quad (12)$$

Hence, the coupling effectively allows a rotation of the measurement axes. For axes given in Eq. (11), we can rewrite Eq. (8) as

$$\begin{aligned} | -\cos(\theta_{\mathbf{a}} + \theta_{\mathbf{b}}) - \cos(\theta_{\mathbf{a}} + \theta_{\mathbf{b}'}) \\ -\cos(\theta_{\mathbf{a}'} + \theta_{\mathbf{b}}) + \cos(\theta_{\mathbf{a}'} + \theta_{\mathbf{b}'}) | \leqslant 2. \end{aligned} \quad (13)$$

Maximal violation of (13) is achieved for example by $\theta_{\mathbf{a}} = 0$, $\theta_{\mathbf{a}'} = \pi/2$, $\theta_{\mathbf{b}} = -\pi/4$, and $\theta_{\mathbf{b}'} = \pi/4$.

The required coupling between $|s\rangle$ and $|p\rangle$ can be provided with microwaves. These would, however, usually couple symmetrically to atoms a and b, which would not allow us to violate (8). To obtain independent control of the pseudospin measurement axes of the two ejected atoms, we require an antisymmetric microwave coupling that could arise on different sides of a field node in an rf resonator as sketched in Fig. 4. Combinations of symmetric ($A_{\text{rf}}^{(+)}$) and antisymmetric ($A_{\text{rf}}^{(-)}$) pulses then can realize the axes necessary for violating the Bell inequality. The example $\theta_{\mathbf{a}} = 0$ with $\theta_{\mathbf{b}'} = \pi/4$ is sketched in Fig. 4. Other ways to achieve independent
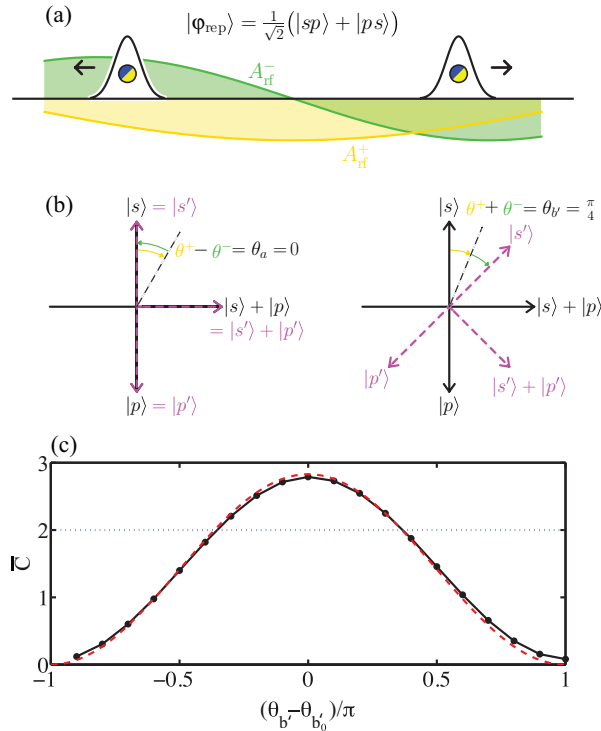
FIG. 4. (Color online) Measurement scheme for atomic pseudospin EPR correlations. (a) Atoms are ejected toward different sides of a microwave node, realizing either same or opposite sign Rabi coupling between $|s\rangle$ $|p\rangle$. (b) Cuts through the Bloch sphere. Combining symmetric and antisymmetric coupling, we can rotate the measurement basis differently for atoms a and b. (c) Correlations $\bar{C}(\theta'_b)$ according to Eq. (8), for fixed $\theta_{a,b,a'}$ (see text) are shown as black (●). Optimal results from Eq. (13) are shown as a red dashed line. The classical limitation $\bar{C} = 2$ is shown as a blue-dotted line.

measurement axes on atoms a and b is to shelve one of the atoms into ground states $|g\rangle$ and $|h\rangle$ for the duration of microwave coupling, and thus coupling $|s\rangle$ to $|p\rangle$ for the remaining Rydberg atom only, or employing a double off-resonant Raman transition that can address an individual atom through laser focusing.

To illustrate the scheme, we modeled the symmetric and and antisymmetric rf pulses coupling $|s\rangle$ and $|p\rangle$ subsequent to atom-pair ejection shown in Fig. 3. A symmetric pulse of 10 ns duration is added at $t = 10.05$ μs, followed

by an asymmetric one at $t = 10.15$ μs. Since ejected atoms are separated by ~10 μm, while microwave lengths are about three orders of magnitude larger, we take the Rabi frequency for the symmetric pulse constant in space, and that for the antisymmetric one linearly varying as $\Omega_{\mathrm{rf}}(t,r) = \Omega_{\mathrm{rf},0}(t)x/|x_0|$, with atom position x, where x_0 is a reference length matching the center of the ejected atom wave packet.

At $t_{\mathrm{measure}} = 10.3$ μs we then extract the expected correlation signal according to Eq. (8). Using the relation (12) between the $C_T^{(\mathbf{a},\mathbf{b})}$ and the pseudospin state of the atom pair after the microwave pulse $U|\chi\rangle$, we can assemble the terms in $\bar{C}$ and find $C_T^{(\mathbf{a},\mathbf{b})} = |c_{s:s}|^2 + |c_{p:p}|^2 - |c_{s:p}|^2 - |c_{p:s}|^2$, where these populations are extracted after microwave coupling as in Eq. (10) corresponding to angles $\theta_{\mathbf{a}}$ and $\theta_{\mathbf{b}}$. The coefficients $c_{x:y}$ relate to a basis describing the state of the *ejected* atoms only. We finally determine $\bar{C}$ from the successful ejection events only.

Choosing the Rabi-coupling angles $\theta_{\mathbf{a}} = 0, \theta_{\mathbf{a}'} = \pi/2, \theta_{\mathbf{b}} = -\pi/4$ as given above and then scanning $\theta_{\mathbf{b}'}$ over the range $\theta_{\mathbf{b}'} \in [-3\pi/4, 5\pi/4]$ results in the graph shown at the bottom of Fig. 4. The EPR region, where correlations exceed the value 2, is clearly visible. The curve from the simulation slightly deviates from the ideal result, given by Eq. (13), since we take into account an uncertainty of rotation angles θ'_b due to the spatial spread of the ejected atoms.

V. CONCLUSIONS AND OUTLOOK

A pair of ultracold atom clouds, each confined tighter than the Rydberg blockade radius and separated by a distance of the order of the blockade radius, can emit pairs of EPR correlated Rydberg or ground-state atoms on demand. The ejected atoms can be shown to violate a Bell inequality in the Rydberg state space with standard methods. Additionally, the setup provides a pulsed single-atom source. The quantumclassical hybrid method used in this article allows for an elegant way to model blockade, Rydberg excitation, and acceleration by state dependent dipole-dipole forces in a single framework.

[1] T. F. Gallagher, *Rydberg Atoms* (Cambridge University Press, Cambridge, 1994).

[2] M. Saffman, T. G. Walker, and K. Mølmer, Rev. Mod. Phys. **82**, 2313 (2010).

[3] E. Urban, T. A. Johnson, T. Henage, L. Isenhower, D. D. Yavuz, T. G. Walker, and M. Saffman, Nat. Phys. **5**, 110 (2009).

[4] A. Gaëtan, Y. Miroshnychenko, T. Wilk, A. Chotia, M. Viteau, D. Comparat, P. Pillet, A. Browaeys, and P. Grangier, Nat. Phys. **5**, 115 (2009).

[5] D. Jaksch, J. I. Cirac, P. Zoller, S. L. Rolston, R. Côté, and M. D. Lukin, Phys. Rev. Lett. **85**, 2208 (2000).

[6] M. D. Lukin, M. Fleischhauer, R.Côté, L. M. Duan, D. Jaksch, J. I. Cirac, and P. Zoller, Phys. Rev. Lett. **87**, 037901 (2001).

[7] A. K. Mohapatra, M. G. Bason, B. Butscher, K. J. Weatherill, and C. S. Adams, Nat. Phys. **4**, 890 (2008).

[8] S. Sevinçli, N. Henkel, C. Ates, and T. Pohl, Phys. Rev. Lett. **107**, 153001 (2011).

[9] M. Saffman and T. G. Walker, Phys. Rev. A **66**, 065403 (2002).

[10] Y. O. Dudin and A. Kuzmich, Science **336**, 887 (2012).

[11] T. Peyronel, O. Firstenberg, Q. Liang, S. Hofferberth, A. V. Gorshkov, T. Pohl, M. D. Lukin, and V. Vuletic, Nature (London) **488**, 57 (2012).

[12] D. Bohm and Y. Aharonov, Phys. Rev. **108**, 1070 (1957).

[13] A. Einstein, N. Rosen, and B. Podolsky, Phys. Rev. **47**, 777 (1935).

[14] Z. Y. Ou, S. F. Pereira, H. J. Kimble, and K. C. Peng, Phys. Rev. Lett. **68**, 3663 (1992).

[15] C. Silberhorn, P. K. Lam, O. Weiß, F. König, N. Korolkova, and G. Leuchs, Phys. Rev. Lett. **86**, 4267 (2001).

[16] C. Schori, J. L. Sørensen, and E. S. Polzik, Phys. Rev. A **66**, 033802 (2002).

[17] W. P. Bowen, R. Schnabel, P. K. Lam, and T. C. Ralph, Phys. Rev. Lett. **90**, 043601 (2003).

[18] A. S. Villar, L. S. Cruz, K. N. Cassemiro, M. Martinelli, and P. Nussenzveig, Phys. Rev. Lett. **95**, 243603 (2005).

[19] J. Jing, S. Feng, R. Bloomer, and O. Pfister, Phys. Rev. A **74**, 041804(R) (2006).

[20] E. Hagley, X. Maitre, G. Nogues, C. Wunderlich, M. Brune, J. M. Raimond, and S. Haroche, Phys. Rev. Lett. **79**, 1 (1997).

[21] M. A. Rowe, D. Kielpinski, V. Meyer, C. A. Sackett, W. M. Itano, C. Monroe, and D. J. Wineland, Nature (London) **409**, 791 (2001).

[22] C. Gross, H. Strobel, E. Nicklas, T. Zibold, N. Bar-Gill, G. Kurizki, and M. K. Oberthaler, Nature (London) **480**, 219 (2011).

[23] K. V. Kheruntsyan, M. K. Olsen, and P. D. Drummond, Phys. Rev. Lett. **95**, 150405 (2005).

[24] R. J. Lewis-Swan and K. V. Kheruntsyan, Phys. Rev. A **87**, 063635 (2013).

[25] M. D. Reid, P. D. Drummond, W. P. Bowen, E. G. Cavalcanti, P. K. Lam, H. A. Bachor, U. L. Andersen, and G. Leuchs, Rev. Mod. Phys. **81**, 1727 (2009).

[26] N. P. Robins, P. A. Altin, J. E. Debs, and J. D. Close, Phys. Rep. **529**, 265 (2013).

[27] S. A. Haine and J. J. Hope, Phys. Rev. A **72**, 033601 (2005).

[28] N. A. Nguyen, B. K. Dey, M. Shapiro, and P. Brumer, J. Chem. Phys. **108**, 7878 (2004).

[29] S. Ospelkaus, K. Ni, D. Wang, M. H. G. de Miranda, B. Neyenhuis, G. Quéméner, P. S. Julienne, J. L. Bohn, D. S. Jin, and J. Ye, Science **327**, 853 (2010).

[30] I. Mourachko, W. Li, and T. F. Gallagher, Phys. Rev. A **70**, 031401 (2004).

[31] W. R. Anderson, J. R. Veale, and T. F. Gallagher, Phys. Rev. Lett. **80**, 249 (1998).

[32] M. Mudrich, N. Zahzam, T. Vogt, D. Comparat, and P. Pillet, Phys. Rev. Lett. **95**, 233002 (2005).

[33] H. Park, E. S. Shuman, and T. F. Gallagher, Phys. Rev. A **84**, 052708 (2011).

[34] T. J. Carroll, K. Claringbould, A. Goodsell, M. J. Lim, and M. W. Noel, Phys. Rev. Lett. **93**, 153001 (2004).

[35] C. S. E. van Ditzhuijzen, A. F. Koenderink, J. V. Hernández, F. Robicheaux, L. D. Noordam, and H. B. van Linden van den Heuvell, Phys. Rev. Lett. **100**, 243201 (2008).

[36] C. Ates, A. Eisfeld, and J.-M. Rost, New J. Phys. **10**, 045030 (2008).

[37] S. Wüster, C. Ates, A. Eisfeld, and J.-M. Rost, Phys. Rev. Lett. **105**, 053004 (2010).

[38] S. Möbius, S. Wüster, C. Ates, A. Eisfeld, and J.-M. Rost, J. Phys. B **44**, 184011 (2011).

[39] C. Ates, T. Pohl, T. Pattard, and J.-M. Rost, Phys. Rev. Lett. **98**, 023002 (2007).

[40] J. C. Tully and R. K. Preston, J. Chem. Phys. **55**, 562 (1971).

[41] J. C. Tully, J. Chem. Phys. **93**, 1061 (1990).

[42] J. S. Bell, Physics **1**, 195 (1964).

[43] J. F. Clauser, M. A. Horne, A. Shimony, and R. A. Holt, Phys. Rev. Lett. **23**, 880 (1969).

[44] S. Möbius, M. Genkin, S. Wüster, A. Eisfeld and J.-M. Rost, Phys. Rev. A **88**, 012716 (2013).

[45] S. Möbius, M. Genkin, A. Eisfeld, S. Wüster, and J.-M. Rost, Phys. Rev. A **87**, 051602(R) (2013).

[46] M. Genkin, S. Wüster, S. Möbius, A. Eisfeld, and J.-M. Rost, arXiv:1308.5864.

[47] S. E. Anderson, K. C. Younge, and G. Raithel, Phys. Rev. Lett. **107**, 263001 (2011).

[48] H. Park, P. J. Tanner, B. J. Claessens, E. S. Shuman, and T. F. Gallagher, Phys. Rev. A **84**, 022704 (2011).

[49] J. C. Tully, Faraday Discuss. **110**, 407 (1998).

[50] S. Hammes-Schiffer and J. C. Tully, J. Chem. Phys. **101**, 4657 (1994).

[51] I. I. Beterov, D. B. Tretyakov, V. M. Entin, E. A. Yakshina, I. I. Ryabtsev, C. MacCormick, and S. Bergamini, Phys. Rev. A **84**, 023413 (2011).

[52] The laser coupling has temporal profiles $\Omega_{las}(t) = \sum_n A_{las} \exp[-(t-t_{0,las,n})^2/(2\tau_{las}^2)]$ and $\Delta_{las}(t) = \sum_n \theta(\tau_{det} - |t-t_{0,las,n}|)[\Delta_{las,-} + (\Delta_{las,+} - \Delta_{las,-})(t - t_{0,las,n} - \tau_{det})/(2\tau_{det})]$, where $\Delta_{las,\pm}$ are the maximal and minimal detuning. Parameters for the laser coupling were $A_{las} = (2\pi)2$ MHz, $t_{0,las,0} = 9$ μs, $t_{0,las,0} = 59$ μs, $\tau_{las} = 2.5$ μs, $\tau_{det} = \tau_{las}$, $\Delta_{las,-} = -(2\pi)8.4$ MHz, and $\Delta_{las,+} = (2\pi)3.3$ MHz. rf pulse shapes in the next section are more complicated. They are displayed in Figs. 3(d) and 3(e), where the maximal detuning (Rabi frequency) was $(2\pi)500$ MHz [$(2\pi)20$ MHz].

[53] We assume an acceleration time $\tau_{acc} = \sqrt{2M/3}d^{5/2}/\mu$, and a drift time $\tau_{drift} = L/v_{fin}$, $v_{fin} = \sqrt{2\mu^2/(Md^3)}$, all from Newton's equations. The drift length of the atoms L is dependent on the experimental setup and set to $L \approx 2d$ here. We estimate the drift velocity as $v_{fin} = a(d)\tau_{acc}$, where $a(d) = 3\mu^2/d^4/M$ is the initial acceleration. In our estimates we use the scaling law $\mu = \mu_0\nu^2$ for the transition dipole, with $\mu_0 = 0.94/\sqrt{3}$ a.u., extrapolating from the reference value $\mu = 966/\sqrt{3}$ a.u. for $\nu = 32$ [69]. Lifetimes of a Rydberg pair state $|sp\rangle$, including the effect of black-body radiation, are calculated as $\tau_{life} = (1/\tau_s + 1/\tau_p)^{-1}$, with $\tau_{s/p} = \tau_{0s/p}\nu^3$ and $\tau_{0s} = 0.48$ ns, $\tau_{0p} = 0.61$ ns [54].

[54] I. I. Beterov, I. I. Ryabtsev, D. B. Tretyakov, and V. M. Entin, Phys. Rev. A **79**, 052504 (2009).

[55] A. Walz-Flannigan, J. R. Guest, J. H. Choi, and G. Raithel, Phys. Rev. A **69**, 063405 (2004).

[56] A. Reinhard, T. Cubel Liebisch, K. C. Younge, P. R. Berman, and G. Raithel, Phys. Rev. Lett. **100**, 123007 (2008).

[57] J. Preclikova, A. Waheed, D. Fregenal, Ø. Frette, B. Hamre, B. T. Hjertaker, E. Horsdal, I. Pilskog, and M. Førre, Phys. Rev. A **85**, 043416 (2012).

[58] S. Wüster, C. Ates, A. Eisfeld, and J.-M. Rost, New J. Phys. **13**, 073044 (2011).

[59] At the given distance, the dipole-dipole force for the pair state $|sp\rangle$ is about 20 times stronger than the van der Waals force for the pair state $|ss\rangle$, which is created in the first step of our scheme (cf. Sec. III A). In the time span between the creation of the $|ss\rangle$ state and the excitation of the repulsive exciton, the van der Waals-induced motion can shift the atoms by about

$\sim 0.03\ \mu$m $\approx 0.1\sigma$, which is insignificant and hence neglected in our simulations.

[60] E. Altiere, D. P. Fahey, M. W. Noel, R. J. Smith, and T. J. Carroll, Phys. Rev. A **84**, 053431 (2011).

[61] T. Vogt, M. Viteau, J. Zhao, A. Chotia, D. Comparat, and P. Pillet, Phys. Rev. Lett. **97**, 083003 (2006).

[62] I. I. Ryabtsev, D. B. Tretyakov, I. I. Beterov, V. M. Entin, and E. A. Yakshina, Phys. Rev. A **82**, 053409 (2010).

[63] J. C. Howell, R. S. Bennink, S. J. Bentley, and R. W. Boyd, Phys. Rev. Lett. **92**, 210403 (2004).

[64] J. Hald, J. L. Sørensen, C. Schori, and E. S. Polzik, Phys. Rev. Lett. **83**, 1319 (1999).

[65] A. Schwarzkopf, R. E. Sapiro, and G. Raithel, Phys. Rev. Lett. **107**, 103001 (2011).

[66] B. Olmos, W. Li, S. Hofferberth, and I. Lesanovsky, Phys. Rev. A **84**, 041607(R) (2011).

[67] G. Günter, M. Robert-de-Saint-Vincent, H. Schempp, C. S. Hofmann, S. Whitlock, and M. Weidemüller, Phys. Rev. Lett. **108**, 013002 (2012).

[68] A. O. Barut and M. Božić, Nuovo Cimento **101**, 595 (1988).

[69] S. Westermann, T. Amthor, A. de Oliveira, J. Deiglmayr, M. Reetz-Lamour, and M. Weidemüller, Eur. Phys. J. D **40**, 37 (2006).